Observed Impacts of Duration and Seasonality of Atmospheric-River Landfalls on Soil Moisture and Runoff in Coastal Northern California

F. M. RALPH

Physical Sciences Division, NOAA/ESRL, Boulder, Colorado

T. COLEMAN

Physical Sciences Division, NOAA/ESRL, and CIRES, Boulder, Colorado

P. J. NEIMAN AND R. J. ZAMORA

Physical Sciences Division, NOAA/ESRL, Boulder, Colorado

M. D. DETTINGER

Scripps Institution of Oceanography, University of California, San Diego, and U.S. Geological Survey, La Jolla, California

(Manuscript received 18 May 2012, in final form 10 October 2012)

ABSTRACT

This study is motivated by diverse needs for better forecasts of extreme precipitation and floods. It is enabled by unique hourly observations collected over six years near California's Russian River and by recent advances in the science of atmospheric rivers (ARs). This study fills key gaps limiting the prediction of ARs and, especially, their impacts by quantifying the duration of AR conditions and the role of duration in modulating hydrometeorological impacts. Precursor soil moisture conditions and their relationship to streamflow are also shown. On the basis of 91 well-observed events during 2004–10, the study shows that the passage of ARs over a coastal site lasted 20 h on average and that 12% of the AR events exceeded 30 h. Differences in storm-total water vapor transport directed up the mountain slope contribute 74% of the variance in storm-total rainfall across the events and 61% of the variance in storm-total runoff volume. ARs with double the composite mean duration produced nearly 6 times greater peak streamflow and more than 7 times the storm-total runoff volume. When precursor soil moisture was less than 20%, even heavy rainfall did not lead to significant streamflow. Predicting which AR events are likely to produce extreme impacts on precipitation and runoff requires accurate prediction of AR duration at landfall and observations of precursor soil moisture conditions.

1. Introduction

Past studies have shown that atmospheric rivers (ARs), which are regions of the lower atmosphere characterized by strong winds and large water vapor contents (usually associated with a surface cold front in the midlatitudes), are key features of the global water cycle (e.g., Zhu and Newell 1998), are detectable in satellite observations (see example in Fig. 1a) (Ralph et al. 2004; Neiman et al. 2008a), and are associated with heavy rain and flooding on the U.S. West Coast (Ralph et al. 2005, 2006, 2011; Neiman et al. 2008b, 2011; Leung and Qian 2009; Smith et al. 2010; Dettinger et al. 2011, 2012; Ralph and Dettinger 2012; White et al. 2012). A useful set of criteria was developed by Ralph et al. (2004) to identify AR conditions in satellite observations at a single time over a broad geographic area in the midlatitudes, based on vertically integrated water vapor (IWV); that is, an area with IWV > 2 cm had to be no more than 1000 km wide and at least 2000 km long. Studies in Europe (Stohl et al. 2008; Lavers et al.

Corresponding author address: Dr. F. Martin Ralph, Physical Sciences Division, NOAA/ESRL, 325 Broadway, Boulder, CO 80305.
E-mail: marty.ralph@noaa.gov

DOI: 10.1175/JHM-D-12-076.1

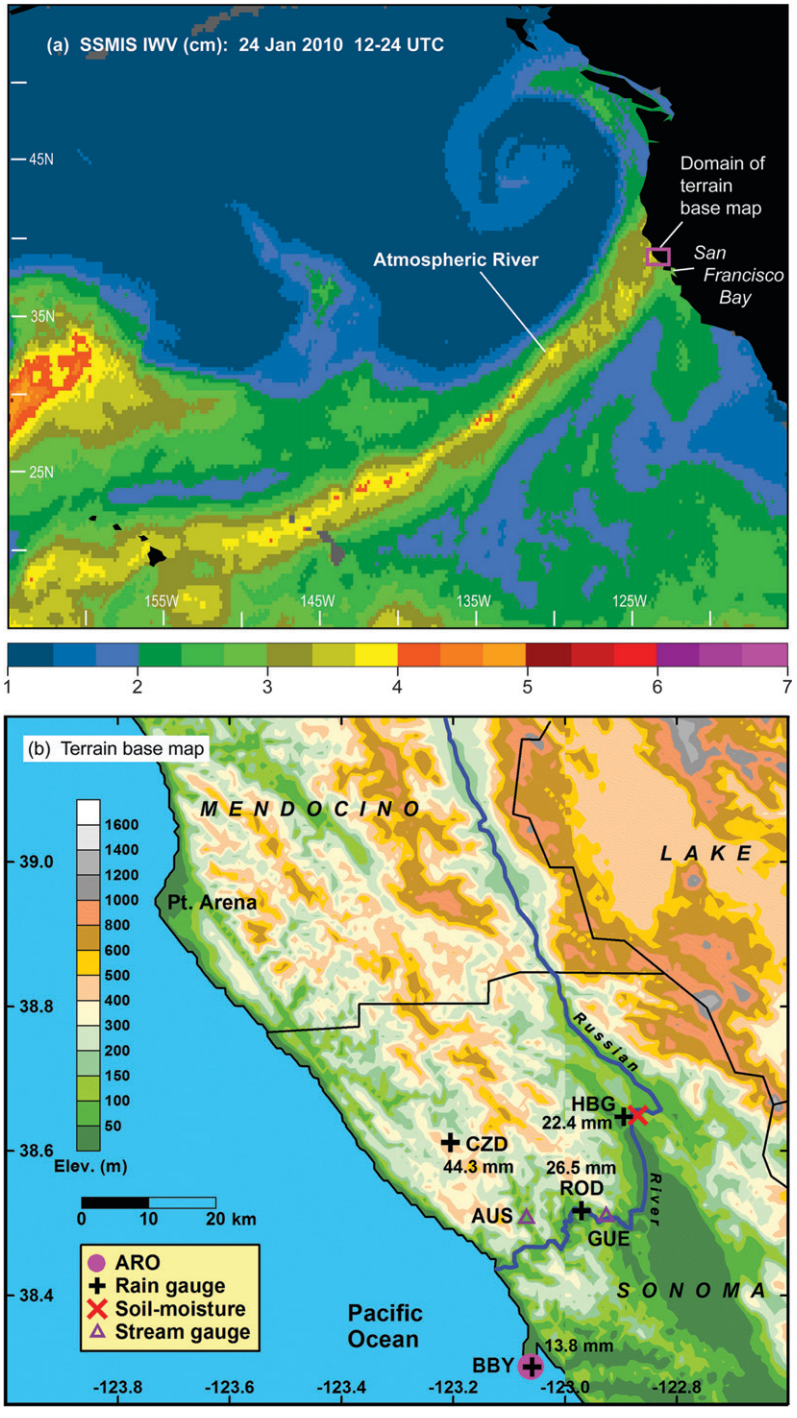

FIG. 1. (a) Satellite image of an AR over the eastern Pacific Ocean seen in IWV. Land is black since SSM/I is not useable over land. The center of the AR's parent extratropical cyclone is evidenced by the curled-up area of enhanced IWV off the Pacific Northwest coast. The AR is striking the observing area (purple box) in California, is one of the long-duration AR events studied, and created the peak streamflow on Austin Creek for water-year 2010. (b) Terrain base map of Northern California's Russian River watershed [see box in (a)] showing the locations of the observing systems, including the ARO at Bodega Bay (see key). The three-letter station names are given for the four experimental sites (see section 2) and USGS stream gauges at AUS and GUE. The numerical values represent composite mean rainfall accumulation associated with the 91 atmospheric rivers documented by the ARO at Bodega Bay. Counties are shown.

2011) and South America (Viale and Nuñez 2011) have come to similar conclusions for the west coasts of these other continents as well, and Moore et al. (2012) has documented the role of an AR in major flooding in the southeast United States. Guan et al. (2010) and Dettinger et al. (2011) documented the major roles that ARs also play in California's water supply, providing from 25% to 50% of the entire water-year's precipitation in just a few events. Finally, Dettinger (2011) analyzed Intergovernmental Panel on Climate Change Fourth Assessment Report (IPCC AR4) climate projections to assess changes in AR characteristics off the California coast and showed that recent climate change projections typically include more extreme ARs in the twenty-first century due largely to greater atmospheric water vapor content.

Despite significant advances in physical understanding of ARs, no systematic assessment of the role of the duration of landfalling AR conditions on hydrometeorological impacts has been conducted, nor has the modulating role of precursor soil moisture on streamflow in AR events been documented. Because ARs usually move across a given location in less than a day and because it is winds at roughly 1 km above ground that are critical to identifying AR conditions (Ralph et al. 2006), neither the standard surface observing network nor the standard 12-hourly upper-air balloon sounding network is capable of monitoring the onset and cessation of AR conditions. Hourly observations aloft are required (e.g., Ralph et al. 2003, 2011; Neiman et al. 2002, 2009) and are being provided by the National Oceanic and Atmospheric Administration's Hydrometeorology Testbed (HMT) (http://hmt.noaa.gov/) (Ralph et al. 2005) operated in California. Key measurements are the hourly upslope wind speed at about 1 km aloft and the vertically integrated water vapor, which, when combined, represent a measure of the critical transport rates of water vapor up mountain slopes. An example of the data aloft is shown in Fig. 2, which is the same case illustrated by the satellite image in Fig. 1a. When the upslope wind from a wind profiler is combined with GPS-Met–derived IWV, roughly 55% of the variance of hourly rain rate in the coastal mountains can be explained (Neiman et al. 2009), indicative of the orographic nature of the precipitation.

Given the inherent rarity of extreme events, it is normally difficult to overcome sample size limitations for research on extreme events. However, this study takes advantage of a 6-yr time series of the HMT observations, which captured 91 AR events, 10 of which are identified as extreme. Eight of these reached extreme rainfall category 1 [RCat 1; as defined in Ralph and Dettinger (2012)], and several produced flooding in the region. It is noteworthy that the region studied here experiences extreme three-day precipitation amounts as large as anywhere else in the contiguous United States, including those associated with landfalling tropical storms and hurricanes in coastal regions and severe convection in the Great Plains (Ralph and Dettinger 2012).

The analysis below is motivated by the need to better understand and predict storm total rainfall and streamflow over several hours to several days in extreme events. To do so, the analysis bridges the fields of meteorology and hydrology. Extreme precipitation forecasts are often low by a factor of 2 in the region partly because weather prediction models do not adequately represent key AR characteristics (Ralph et al. 2010), including landfall duration, and the cloud and precipitation microphysical processes in AR events (Jankov et al. 2009).

2. Data and methodology

This study uses unique observations collected in the vicinity of the Russian River basin northwest of San Francisco, California, for the six years between 13 November 2004 and 8 August 2010 (Fig. 1b) in support of the Hydrometeorology Testbed (HMT). The cornerstone observing platform was an atmospheric river observatory (ARO; White et al. 2012) on the coast at Bodega Bay (BBY, 12 m MSL). The ARO consisted of a 915-MHz wind profiler, a GPS receiver, and a suite of surface meteorological instruments. The wind profiler (e.g., Carter et al. 1995) provided hourly averaged vertical profiles of horizontal wind velocity from ~0.1 to 4 km above ground with ~100-m vertical resolution and ~1 m s^{-1} accuracy in all weather conditions (see example in Fig. 2a). Measurements of IWV in the full atmospheric column were retrieved half-hourly with ~1-mm accuracy from the GPS receiver by measuring delays in the arrival of radio signals transmitted by the constellation of GPS satellites (e.g., Duan et al. 1996; Mattioli et al. 2007). In addition to other parameters, at the surface a tipping-bucket gauge measured 2-min accumulated rainfall with 0.01-inch (0.254 mm) accuracy. Surface meteorological data from three additional sites are also used: Cazadero in the coastal mountains (CZD, 475 m MSL), Rio Nido in the lower Russian River basin (ROD, 30 m MSL), and Healdsburg in the middle Russian River basin (HBG, 62 m MSL). The HBG site included a probe to record soil moisture at 10 cm below the surface (Zamora et al. 2011). Streamflow series from two U.S. Geological Survey (USGS) gauges were analyzed, one at Guerneville (GUE, 3465-km^2 drainage area) on the lower Russian

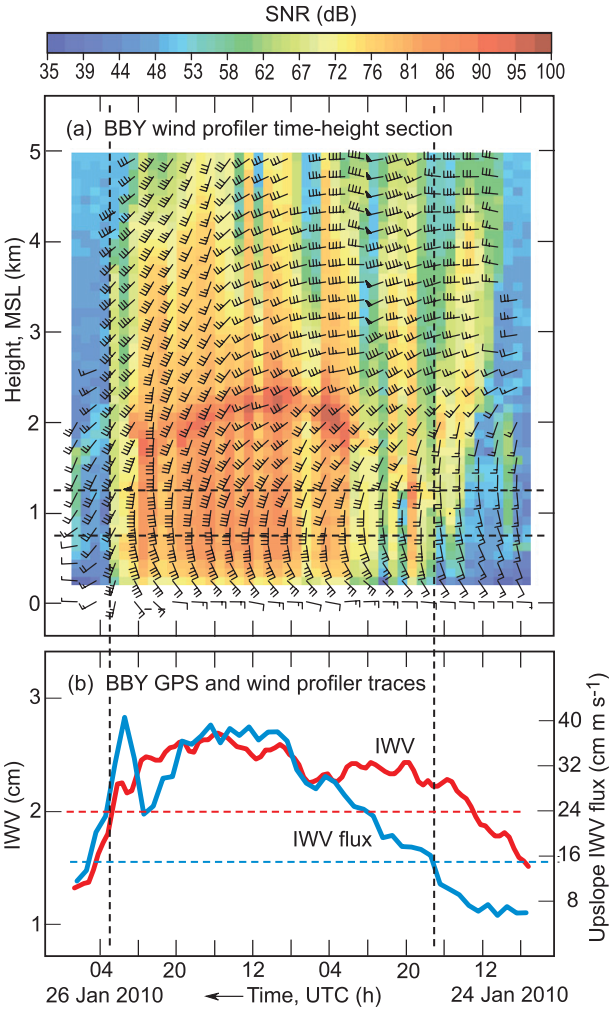

FIG. 2. (a) Time–height cross section of winds aloft measured using the BBY radar wind profiler. Time is reversed based on a meteorological plotting convention for such data. Dashed horizontal lines denote the range of altitudes of the "controlling layer" (Neiman et al. 2002) over which horizontal winds are averaged to calculate the upslope wind speed. Color fill represents the signal-to-noise ratio of the backscattered energy observed by the radar. Warm colors (yellow, orange, and red) correspond to periods when precipitation was present. (b) Time series of IWV derived from a collocated GPS-Met site (red) and upslope IWV flux (blue). Horizontal dashed red and blue lines are the threshold values used to determine when AR conditions are present. Vertical dashed lines across both panels represent the start and end time of AR conditions based on the thresholds used in this study.

River and the other on Austin Creek (AUS, 163 km^2), which feeds into the Russian River downstream of GUE. Austin Creek is a small basin adjacent to the CZD drainage (Fig. 1b). Finally, daily precipitation totals from the Cooperative Observer (COOP) rain gauge network at five sites within 40 km of CZD are used.

In the initial step to gauge the impact of orographic forcing on precipitation generation and, ultimately, on soil moisture and streamflow responses, the upslope component of the winds measured by the BBY wind profiler in a 500-m-thick orographic controlling layer centered at 1 km MSL was determined hourly [see Neiman et al. (2002) for the detailed methodology and motivation of using this approach]. Given that the mean orientation of the crest of the coastal mountains here is along ~140°–320°, the upslope component is directed from 230°. Using these data, the terrain-perpendicular water vapor flux centered at 1 km MSL was approximated hourly by calculating the product of the simultaneously measured upslope wind in that layer and the IWV [see Neiman et al. (2009) for more details]. This variable is referred to hereinafter as the upslope IWV flux. Although the IWV is column integrated, water vapor is typically concentrated in the lower troposphere.[1] Hence, to first order, the temporal variability of IWV reflects changes in water vapor in the lower troposphere, such that this upslope IWV flux provides a practical estimate of the lower-altitude water vapor transport into the mountains.

Using these data, 103 possible AR events were identified based on three thresholds: 1) the IWV had to meet or exceed 2 cm [as in Ralph et al. (2004) and subsequent studies], 2) the upslope IWV flux had to meet or exceed 15 cm (m s^{-1}) (which was well correlated with the onset of significant precipitation at CZD), and 3) both variables had to simultaneously meet or exceed those thresholds for at least eight consecutive hours [the same minimum duration criterion was applied in earlier meteorological studies in the region; Neiman et al. (2002, 2010)]. Twelve of these cases were continuations of previous ARs, reducing the total number of distinct cases to 91. Each case was then represented in the following analyses by a 96-h time interval with the 24th hour arranged, in each case, to be the start of the period for which IWV $\geq$ 2 cm and upslope IWV flux $\geq$ 15 cm (m s^{-1}) for at least 8 h. Key parameters for each of the 91 cases are shown in Table 1, including start and end dates and times, as well as many key variables representing the meteorological forcing and hydrological impacts.

The method used to create this set of dates and times complements the satellite-based method of detecting ARs in IWV observed offshore using the Special Sensor Microwave Imager (SSM/I) (Ralph et al. 2004; Neiman

[1] Based on the DJF mean vertical profile of water vapor specific humidity for the Northern Hemisphere (Peixoto and Oort 1992), the layer below 700 hPa (800 hPa) contains ~80% (60%) of the seasonal hemispheric average IWV.

et al. 2008b). The satellite-based methods have 12-hourly sampling, rather than the hourly sampling used here, and do not have the advantage of incorporating wind observations aloft from the radar wind profiler. Another important distinction is that the satellite-based method uses observations at a single time over a broad geographic area to assess the criteria of maximum width scale (<1000 km wide area of IWV > 2 cm) and minimum length scale (IWV > 2 cm is present along an axis >2000 km long) defined in Ralph et al. (2004), whereas this study uses a time series of essentially point data as an atmospheric river passes overhead. Thus, it is to be expected that some AR cases would be detected with the wind-profiler-based approach used here that were not detected in the satellite-based approach and vice versa. The approaches are highly complementary in that one focuses offshore and one at the coast, and one infers water vapor transport from IWV spatial patterns while the other measures water vapor transport from a point.

3. Results

a. All cases

A total of 1460 h met the atmospheric-river criteria during the 91 cases. During these hours, which correspond to only 2.8% of all hours in the nearly 6-yr-long time series, CZD accumulated 51% (4618 mm) of all rain measured at that site (9107 mm). This fraction is similar to the values found by Dettinger et al. (2011) using an independent set of daily data (not hourly as in this study) including AR dates from satellite and daily rainfall data from many COOP sites in Northern California. Of the 91 cases, 80 corresponded to dates of AR conditions based on SSM/I satellite observations offshore of California (Neiman et al. 2008b).[2] [As described in section 2, the approach used here is based on a relatively direct measurement of water vapor transport from a point at the coast versus inferring transport from IWV spatial patterns offshore (Ralph et al. 2004; Neiman et al. 2008b).] Applying the Dettinger et al. (2011) methodology to five COOP stations nearest CZD for the same six years revealed that 41% of total precipitation was associated with landfalling ARs. Regarding streamflow, the top 1% of hourly flows on Austin Creek represented 503 h over the nearly six years. Of these 503 h of highest flows, 90% occurred within 72 h of the start of AR conditions in the 91 events.

Based on the composite of all 91 cases (Table 2, Fig. 3), the ''composite average'' duration of AR conditions was 20 h.[3] During this 20 h, on average, 44 mm of rain fell at CZD, soil moisture increased from 29% to 35% volumetric water content (VWC; Zamora et al. 2011), and streamflow increased on Austin Creek from 5.7 to 31.6 $m^3 s^{-1}$ (hereafter cms) and on the Russian River from 55.6 to 159.5 cms (a factor of 5.3 and 2.8, respectively). When only those events with at least 45 mm of precipitation are considered (60 events), the average duration was 29 h (Table 2). More so than the effects of increased maximum upslope IWV flux (7%) and average rain rates (16%), it is the 45% longer duration that led to a 68% increase in storm-total rainfall for this subset of cases (Table 2). The difference between 29% and 35% VWC represents a saturation excess. The maximum volume of water that can be stored in the soil is approximately 29% or field capacity. The additional 6% VWC cannot be stored in the soil and that amount of water is available for runoff.

During AR conditions the maximum hourly values of IWV, upslope wind, and upslope IWV flux averaged 2.69 cm, 12.8 m s^{-1}, and 32.5 cm (m s^{-1}) (Fig. 3). The 91 AR cases included all six of the dates of annual peak daily streamflows at Austin Creek for water-year (WY) 2005–10 (e.g., the case shown in Fig. 1a is the event that created the peak streamflow on Austin Creek for WY 2010, that is, 288.7 cms on 25 January 2010). All of these dates also corresponded to AR dates in the SSM/I satellite-based AR catalog of Neiman et al. (2008a).

In addition to the mean values of the major forcing parameters, it is useful to document the frequency of occurrence of values of each variable during AR conditions. For this purpose, Fig. 4 shows histograms of hourly IWV, upslope wind speed, and upslope IWV flux values for the 1460 h of AR conditions contained in the 91 AR events. Table 3 documents the thresholds defining the top 1% and top 10% of hourly values within

[2] The 11 events that still do not overlap were not identified in satellite data as AR events because either 1) the 2-cm threshold was not fully met (in this case the structure of an AR was present, but it was slightly below the 2-cm threshold) or 2) the area of >2 cm exceeded the 1000-km-wide criteria. In the latter case, it is likely that AR conditions were embedded in the broader area of larger water vapor contents, which is suggested by some of the structure seen in these satellite images.

[3] The ''composite average'' duration of 20 h used here is based on the single composite time series, which is derived by averaging the values of each variable using the same storm-relative hour and then doing this for each of the 96 h used. For comparison, the arithmetic average of duration can be calculated using the total hours of AR conditions summed for all 91 cases and then dividing by 91. This yields 16 h as the average duration.

TABLE 1. Meteorological and hydrological characteristics of each of the 91 ARs. The column entries are AR start date and time (1), AR end date and time (2), AR duration (3), Composite season (4), Hours after previous event as AR specific hours (5), SSM/I AR landfalls in California in the morning or afternoon (6), CZD accumulated precipitation (7), BBY max IWV (8), BBY max upslope wind speed between 0.75 and 1.25 km MSL (9), BBY wind direction between 0.75 and 1.25 km MSL (10), BBY max upslope IWV flux between 0.75 and 1.25 km MSL (11), BBY storm-total upslope IWV flux between 0.75 and 1.25 km MSL (12), CZD average rain rate (13), CZD max hourly rain rate (14), HBG min/max soil moisture (15), Min/max discharge: Austin Creek (16), and Min/max discharge: Russian River (17).

(1) (UTC)	(2) (UTC)	(3) (h)	(4) (months)	(5) (h)	(6) (day −1, 0, 1)	(7) (mm)	(8) (cm)	(9) (m s^{-1})	(10) (deg)	(11) [cm (m s^{-1})]	(12) [cm (m s^{-1})]	(13) (mm h^{-1})	(14) (mm h^{-1})	(15) (%)	(16) (cms)	(17) (cms)
0500 27 Nov 2004	1400 27 Nov 2004	9	SON		0	28.4	3.19	19.8	246.8	63.3	356	3.2	13.0	26.1/31.8	0.3/1.0	6.4/6.4
2000 6 Dec 2004	0800 7 Dec 2004	12	DJF	223	0	90.4	2.58	29.2	211.7	75.2	579	7.5	11.9	29.3/53.4	0.3/151.5	6.6/101.9
0000 8 Dec 2004	0800 9 Dec 2004	32	DJF	17	0	87.4	3.15	22.0	232.7	59.9	1044	2.7	11.2	37.4/47.2	5.7/176.2	60.8/362.2
1200 25 Jan 2005	1300 26 Jan 2005	25	DJF	1133		40.4	2.52	11.9	176.4	29.3	518	1.6	6.9	35.8/50.0	2.3/7.2	29.4/47.8
0400 19 Mar 2005	1600 19 Mar 2005	12	MAM	1239	0	42.7	2.67	15.0	191.9	39.1	364	3.6	8.6	29.6/46.7	4.6/70.5	25.6/68.5
0100 22 Mar 2005	1000 22 Mar 2005	9	MAM	58	1	27.2	2.72	23.1	198.8	59.7	347	3.0	7.6	46.9/48.7	17.5/180.9	189.6/319.8
1900 27 Mar 2005	0400 28 Mar 2005	9	MAM	130	0	43.9	2.80	20.2	197.7	54.8	348	4.9	10.9	34.3/45.0	9.1/76.0	74.1/196.7
0700 8 May 2005	2000 8 May 2005	13	MAM	988	1	33.8	2.87	12.0	205.6	33.1	315	2.6	6.4	28.1/36.8	2.3/8.4	21.7/48.4
1100 15 May 2005	2100 15 May 2005	10	MAM	160	0	0.0	3.88	6.3	271.5	22.7	195	0.0	0.0	29.0/29.4	2.7/2.7	25.4/26.1
2100 17 May 2005	0400 19 May 2005	31	MAM	49	0	172.2	3.68	20.3	211.5	74.5	1364	5.6	15.2	28.1/42.9	2.5/157.8	23.2/356.6
0400 8 Jun 2005	1400 8 Jun 2005	10	JJA	481	1	7.1	3.21	10.0	268.0	30.1	226	0.7	2.0	21.2/21.6	1.6/1.7	0.0/0.0
1500 16 Jun 2005	0000 17 Jun 2005	9	JJA	194	0	22.1	3.22	16.1	215.1	49.1	256	2.5	6.9	20.0/20.6	1.3/2.0	0.0/0.0
2000 17 Jun 2005	0400 18 Jun 2005	8	JJA	21	0	3.0	2.19	8.0	219.8	17.2	130	0.4	2.0	20.8/20.9	1.6/1.6	0.0/0.0
0200 26 Oct 2005	1300 26 Oct 2005	11	SON	3119	1	16.5	2.80	11.4	217.6	31.9	264	1.5	4.6	7.1/7.2	0.1/0.3	5.2/5.3
0100 28 Oct 2005	1900 28 Oct 2005	18	SON	37	0	44.7	2.73	13.2	212.1	34.2	458	2.5	6.1	7.1/16.6	0.2/1.8	5.5/6.3
1900 3 Nov 2005	0800 4 Nov 2005	13	SON	145	0	29.2	2.46	16.6	248.0	37.8	321	2.3	5.8	15.5/15.6	0.1/0.7	6.0/6.3
0600 7 Nov 2005	0200 8 Nov 2005	20	SON	72	0	44.7	3.04	13.2	196.2	36.9	568	2.2	15.2	15.6/25.7	0.3/3.3	71/15.1
0500 25 Nov 2005	1700 25 Nov 2005	12	SON	412	1	28.7	3.55	16.9	245.1	58.9	400	2.4	6.6	22.3/31.1	0.2/0.7	4.6/5.0

TABLE 1. (*Continued*)

(1) (UTC)	(2) (UTC)	(3) (h)	(4) (months)	(5) (h)	(6) (day −1, 0, 1)	(7) (mm)	(8) (cm)	(9) (m s^{-1})	(10) (deg)	(11) [cm (m s^{-1})]	(12) [cm (m s^{-1})]	(13) (mm h^{-1})	(14) (mm h^{-1})	(15) (%)	(16) (cms)	(17) (cms)
2000 28 Nov 2005	1300 29 Nov 2005	17	SON	76	0	27.7	3.12	14.0	196.4	41.5	476	1.6	4.6	27.1/35.5	0.3/6.0	5.7/6.9
2100 30 Nov 2005	0200 2 Dec 2005	29	SON	33	0	112.5	3.24	25.4	235.0	82.2	1275	3.9	13.0	33.4/39.0	1.0/106.1	13.4/174.6
0500 18 Dec 2005	0000 20 Dec 2005	43	DJF	388	0	99.1	3.21	23.5	217.9	67.1	1685	2.3	13.5	31.1/51.4	0.7/108.0	10.6/273.7
1000 20 Dec 2005	0000 21 Dec 2005	14	DJF	11	0	34.8	3.32	16.8	197.1	54.7	448	2.5	9.7	40.0/45.7	7.2/31.6	120.8/182.0
1200 21 Dec 2005	2200 22 Dec 2005	34	DJF	13	0	83.6	3.81	17.2	222.2	54.5	1213	2.5	13.0	43.1/45.5	18.1/112.6	152.5/472.6
1700 25 Dec 2005	0900 26 Dec 2005	16	DJF	68	−1	49.0	2.81	17.8	231.2	40.8	469	3.1	11.2	37.5/44.8	7.3/83.0	90.0/187.9
0700 27 Dec 2005	1700 28 Dec 2005	34	DJF	23	0	168.9	3.58	19.7	237.6	68.7	1544	5.0	17.8	40.9/46.2	15.7/281.2	133.3/897.1
0400 30 Dec 2005	1600 31 Dec 2005	36	DJF	36	0	203.5	3.58	30.4	235.6	103.1	1880	5.7	20.3	41.6/47.3	22.0/485.3	279.6/1624.4
1500 1 Jan 2006	0200 2 Jan 2006	11	DJF	24	0	80.0	2.67	23.2	186.3	60.5	442	7.3	16.0	43.3/47.7	49.6/365.8	769.8/916.9
2100 3 Jan 2006	0600 4 Jan 2006	9	DJF	44	0	47.2	2.19	18.1	208.1	38.3	271	5.3	8.4	45.9/48.0	32.8/80.9	328.3/410.4
2300 10 Jan 2006	0900 11 Jan 2006	10	DJF	162	0	4.8	3.00	9.3	240.0	26.8	225	0.5	1.8	37.6/38.2	7.8/7.9	70.5/72.7
1400 28 Jan 2006	0400 29 Jan 2006	14	DJF	414		50.5	2.56	14.5	234.2	33.8	370	3.6	9.1	41.1/45.6	5.2/32.1	64.0/99.3
0900 1 Feb 2006	2100 1 Feb 2006	12	DJF	78	1	32.5	3.08	11.3	264.4	28.7	255	2.7	7.4	44.7/47.8	11.7/21.4	116.6/133.3
1700 26 Feb 2006	0700 28 Feb 2006	38	DJF	597	0	168.7	3.12	20.9	193.8	61.5	1523	4.4	13.7	30.3/48.1	1.5/153.5	0.0/427.3
0800 5 Mar 2006	0500 6 Mar 2006	21	MAM	122	0	105.2	2.52	20.9	187.2	52.0	698	5.0	12.4	44.9/50.0	14.5/186.2	148.3/781.1
0000 12 Apr 2006	1500 12 Apr 2006	15	MAM	883	1	77.2	2.58	15.1	174.2	38.5	416	5.2	9.4	48.7/49.4	59.1/205.6	387.7/642.4
1400 19 May 2006	0900 20 May 2006	19	MAM	888	0	1.8	2.90	12.6	222.9	34.7	429	0.1	0.8	13.9/16.4	1.5/1.6	18.2/18.6
0600 23 May 2006	1400 23 May 2006	8	MAM	70	0	2.3	2.39	9.1	192.0	20.7	137	0.3	0.5	0.0/0.0	1.4/1.5	19.6/19.6
0700 2 Jun 2006	1500 2 Jun 2006	8	JJA	234	0	0.0	3.70	7.6	266.1	28.0	168	0.0	0.0	15.3/16.7	1.0/0.1	12.9/13.1
0700 2 Nov 2006	2100 2 Nov 2006	14	SON	3665	1	21.1	3.35	13.5	209.3	45.1	454	1.5	5.1	9.7/19.9	0.1/0.7	5.5/6.1

TABLE 1. (*Continued*)

(1) (UTC)	(2) (UTC)	(3) (h)	(4) (months)	(5) (h)	(6) (day −1, 0, 1)	(7) (mm)	(8) (cm)	(9) (m s^{-1})	(10) (deg)	(11) [cm (m s^{-1})]	(12) [cm (m s^{-1})]	(13) (mm h^{-1})	(14) (mm h^{-1})	(15) (%)	(16) (cms)	(17) (cms)
0400 8 Nov 2006	1300 8 Nov 2006	9	SON	129	1	2.5	3.57	8.0	253.2	27.8	174	0.3	0.5	16.5/16.6	0.1/0.1	6.1/6.1
0500 13 Nov 2006	0900 14 Nov 2006	27	SON	113	0	38.6	3.67	14.4	227.1	44.2	807	1.4	4.6	18.5/27.5	0.2/1.7	6.7/7.6
0700 16 Nov 2006	1500 16 Nov 2006	8	SON	47	1	10.9	3.31	9.3	255.6	30.6	185	1.4	2.8	24.1/24.4	0.3/0.3	7.2/7.5
0600 21 Nov 2006	1400 21 Nov 2006	8	SON	112	0	0.0	2.66	9.6	255.6	25.6	157	0.0	0.0	23.2/23.2	0.2/0.2	6.1/6.1
2200 8 Dec 2006	0900 9 Dec 2006	11	DJF	417		47.0	2.82	14.3	203.7	40.4	290	4.3	8.9	26.5/37.1	0.2/6.0	6.1/6.4
1500 11 Dec 2006	0500 12 Dec 2006	14	DJF	55	1	35.1	2.94	12.7	229.0	35.3	358	2.5	11.7	35.3/40.1	2.3/37.4	19.2/29.7
0500 13 Dec 2006	0200 14 Dec 2006	21	DJF	23	0	12.2	3.04	10.7	237.4	32.2	423	0.6	1.8	35.7/36.7	4.1/6.4	27.9/48.4
0700 21 Dec 2006	0000 22 Dec 2006	17	DJF	174	0	35.8	2.63	15.5	224.0	40.8	470	2.1	7.1	34.9/42.0	0.6/14.2	12.7/30.6
1300 26 Dec 2006	0200 27 Dec 2006	13	DJF	110	0	92.2	3.12	24.1	210.4	67.8	620	7.1	20.1	35.9/56.7	1.2/161.5	19.0/249.9
2100 3 Jan 2007	1000 4 Jan 2007	13	DJF	188	1	25.9	2.83	12.8	263.0	35.2	294	2.0	5.8	35.8/36.2	2.5/4.6	20.7/21.1
1500 8 Feb 2007	0400 11 Feb 2007	57	DJF	846	0	231.4	3.08	19.9	212.7	55.8	1571	4.1	10.9	39.0/55.1	2.1/209.1	13.2/515.1
2300 21 Feb 2007	0900 22 Feb 2007	10	DJF	260		38.1	2.34	17.5	198.6	40.3	295	3.8	7.6	36.3/52.5	4.6/31.2	25.8/111.8
2200 1 May 2007	1100 2 May 2007	13	MAM	1645	0	7.1	2.88	9.5	254.6	26.9	266	0.6	1.5	19.1/19.3	0.8/0.8	9.1/9.2
0000 18 Jul 2007	0800 18 Jul 2007	8	JJA	1838	0	1.3	4.21	5.7	277.7	24.0	159	0.2	0.5	7.1/7.1	0.1/0.1	4.2/4.3
0700 22 Sep 2007	1900 22 Sep 2007	12	SON	1584		0.0	2.91	10.8	217.4	29.0	255	0.0	0.0	4.9/4.9	0.0/0.0	3.7/3.8
1900 9 Oct 2007	1000 10 Oct 2007	15	SON	409	1	50.5	3.28	18.3	204.6	60.1	420	3.4	12.4	4.7/10.4	0.0/0.2	4.0/4.6
1000 12 Oct 2007	1800 12 Oct 2007	8	SON	49	−1	10.2	2.84	8.9	179.9	23.5	169	1.3	3.0	12.0/13.7	0.1/0.2	4.7/5.0
1400 18 Oct 2007	0800 19 Oct 2007	18	SON	141	0	14.2	3.31	8.3	237.4	26.3	380	0.8	3.3	18.7/18.8	0.3/0.3	4.8/4.9
1900 2 Dec 2007	1300 4 Dec 2007	42	DJF	1069	0	69.3	4.35	15.5	228.8	67.3	1297	1.7	11.4	15.4/28.9	0.1/18.4	4.9/5.9
0200 18 Dec 2007	1900 18 Dec 2007	17	DJF	326	0	86.6	2.54	17.5	221.2	44.5	507	5.1	13.7	32.8/43.8	0.8/121.0	5.0/23.0

TABLE 1. (*Continued*)

(1) (UTC)	(2) (UTC)	(3) (h)	(4) (months)	(5) (h)	(6) (day −1, 0, 1)	(7) (mm)	(8) (cm)	(9) (m s^{-1})	(10) (deg)	(11) [cm (m s^{-1})]	(12) [cm (m s^{-1})]	(13) (mm h^{-1})	(14) (mm h^{-1})	(15) (%)	(16) (cms)	(17) (cms)
2200 19 Dec 2007	1000 20 Dec 2007	12	DJF	28	0	78.0	2.90	21.1	240.3	61.2	417	6.5	16.0	31.9/53.2	8.1/110.9	26.0/69.6
1300 3 Jan 2008	2200 4 Jan 2008	33	DJF	340	1	262.4	3.10	35.9	215.4	109.0	1607	8.0	21.1	31.9/56.3	2.1/397.7	9.8/976.4
0900 10 Jan 2008	1800 10 Jan 2008	9	DJF	132	1	0.0	2.88	10.8	230.6	31.2	226	0.0	0.0	40.2/45.7	15.9/20.8	102.4/111.8
0200 26 Jan 2008	1400 26 Jan 2008	12	DJF	369	0	77.2	2.40	16.3	169.9	38.7	319	6.4	11.7	52.2/54.1	59.2/204.6	0.0/0.0
1900 2 Feb 2008	0700 3 Feb 2008	12	DJF	174	1	88.1	2.43	20.8	232.8	47.1	379	7.3	14.7	43.3/50.5	30.5/122.7	168.1/319.8
1800 28 Mar 2008	0200 29 Mar 2008	8	MAM	1307		4.8	2.29	15.1	224.3	34.0	181	0.6	1.3	14.4/14.4	1.1/1.2	10.2/10.2
0900 2 Oct 2008	1900 2 Oct 2008	10	SON	4496	0	4.1	3.16	10.4	236.7	31.9	203	0.4	2.5	3.3/3.3	0.0/0.0	3.8/3.9
1400 3 Oct 2008	0800 4 Oct 2008	18	SON	20	0	64.8	3.77	17.8	228.2	62.4	643	3.6	17.5	3.3/13.4	0.0/0.3	3.9/5.7
0500 31 Oct 2008	1600 31 Oct 2008	11	SON	646		20.3	2.77	13.7	175.6	37.0	292	1.9	8.4	10.7/18.5	0.0/0.0	4.1/4.9
2300 5 Nov 2008	0700 6 Nov 2008	8	SON	129	−1	2.3	2.96	7.3	247.3	20.2	141	0.3	0.5	30.3/30.5	1.2/1.4	12.8/13.9
1400 21 Dec 2008	0200 22 Dec 2008	12	DJF	1088	0	18.3	2.64	16.4	230.9	40.1	369	1.5	3.8	33.6/38.5	0.7/2.1	9.1/11.3
1300 24 Dec 2008	0900 25 Dec 2008	20	DJF	60	−1	57.9	2.41	22.0	217.0	50.6	573	2.9	15.7	41.8/58.9	1.7/91.1	15.8/55.5
0800 2 Jan 2009	1600 2 Jan 2009	8	DJF	192		22.4	2.44	13.9	272.3	33.0	177	2.8	8.1	34.2/36.3	1.0/1.3	13.8/13.9
0200 22 Feb 2009	0400 23 Feb 2009	26	DJF	1211	0	168.9	2.75	19.1	190.9	50.8	842	6.5	18.5	35.2/52.6	4.1/105.3	58.0/566.0
0900 1 Mar 2009	1900 1 Mar 2009	10	DJF	150	0	13.0	2.69	10.4	170.7	25.3	214	1.3	3.3	35.6/50.2	7.0/9.1	84.1/95.7
2000 15 Mar 2009	0500 16 Mar 2009	9	MAM	337	0	10.2	2.50	9.8	232.1	24.5	175	1.1	2.3	29.1/29.2	3.0/3.1	34.2/35.1
1800 1 May 2009	0400 2 May 2009	10	MAM	1118		31.2	2.94	21.3	208.6	60.6	353	3.1	8.6	13.3/30.7	0.5/1.2	8.1/11.7
1300 2 May 2009	2100 2 May 2009	8	MAM	10		15.7	3.10	10.7	197.3	33.3	188	2.0	5.1	27.4/33.0	1.2/1.4	10.6/11.4
0500 3 May 2009	1500 3 May 2009	10	MAM	9		33.3	3.10	15.7	216.8	48.6	281	3.3	9.4	30.5/35.3	1.6/7.3	12.0/23.9
1200 4 May 2009	1000 5 May 2009	22	MAM	22	0	71.4	3.39	15.8	229.5	52.4	711	3.2	15.0	29.0/34.5	2.5/61.1	21.6/65.7

TABLE 1. (*Continued*)

(1) (UTC)	(2) (UTC)	(3) (h)	(4) (months)	(5) (h)	(6) (day −1, 0, 1)	(7) (mm)	(8) (cm)	(9) (m s^{-1})	(10) (deg)	(11) [cm (m s^{-1})]	(12) [cm (m s^{-1})]	(13) (mm h^{-1})	(14) (mm h^{-1})	(15) (%)	(16) (cms)	(17) (cms)
1100 6 May 2009	2100 6 May 2009	10	MAM	26	0	5.8	2.84	11.7	253.8	32.6	237	0.6	1.5	30.4/30.9	6.4/7.8	58.6/71.0
0200 13 Oct 2009	0200 14 Oct 2009	24	SON	3822	0	134.1	3.59	21.9	219.2	76.5	982	5.6	17.3	3.2/36.4	0.1/22.2	4.7/24.4
1300 15 Dec 2009	0000 16 Dec 2009	11	DJF	1501	0	0.5	2.34	10.0	193.4	20.8	203	0.1	0.5	34.8/35.4	1.3/1.5	14.0/14.8
0500 1 Jan 2010	2200 1 Jan 2010	17	DJF	376	0	24.9	2.60	12.7	219.1	33.0	377	1.5	7.9	37.8/55.4	1.3/8.9	11.6/14.3
0500 12 Jan 2010	1600 12 Jan 2010	11	DJF	248	1	69.6	2.92	21.2	210.4	55.0	451	6.3	12.7	35.6/53.6	0.8/68.2	12.6/49.0
2000 17 Jan 2010	0500 18 Jan 2010	9	DJF	125	1	62.7	2.22	20.5	209.1	42.6	315	7.0	15.5	43.0/52.6	5.3/75.8	27.6/72.4
1700 24 Jan 2010	0300 26 Jan 2010	34	DJF	157	0	109.7	2.68	18.4	195.1	40.6	1017	3.2	8.6	47.5/57.2	17.5/279.1	212.0/860.3
1600 4 Feb 2010	0500 5 Feb 2010	13	DJF	230	0	57.2	2.56	20.5	180.8	49.2	410	4.4	11.7	37.2/54.6	3.7/118.5	69.3/204.0
1400 12 Mar 2010	2300 12 Mar 2010	9	MAM	850	0	57.2	2.55	17.3	223.4	44.0	270	6.4	9.9	37.6/51.4	5.5/50.9	71.3/113.5
0200 29 Mar 2010	2000 29 Mar 2010	18	MAM	387	0	2.5	2.69	12.8	238.8	33.7	462	0.1	1.5	25.7/26.1	1.9/4.1	33.1/34.0
1300 2 Apr 2010	2200 2 Apr 2010	9	MAM	90	1	46.2	2.45	16.7	241.4	39.3	281	5.1	10.9	38.5/50.1	6.5/26.0	75.6/86.0
0500 27 Apr 2010	1700 27 Apr 2010	12	MAM	584	1	55.9	3.15	16.5	224.4	52.0	477	4.7	9.7	25.3/36.0	3.5/16.4	45.8/52.1
1600 19 May 2010	0000 20 May 2010	8	MAM	528	0	4.8	2.83	12.6	233.8	31.2	207	0.6	1.5	24.8/25.6	2.0/2.0	26.5/27.2

TABLE 2. Mean characteristics of composites of AR events, including sensitivity to duration and season. Values are extracted from the composites during AR conditions only except for soil moisture and river discharge, which are from any time within the 96-h composite time window. Column entries are composites (number of ARs) (1), AR duration (2), CZD accumulated precipitation during AR hours (3), BBY max IWV (4), BBY max upslope wind speed between 0.75 and 1.25 km MSL (5), BBY wind direction between 0.75 and 1.25 km MSL (6), BBY max upslope IWV flux between 0.75 and 1.25 km MSL (7), BBY AR storm-total upslope IWV flux between 0.75 and 1.25 km MSL (8), CZD average rain rate (9), CZD max hourly rain rate (10), HBG min/max soil moisture (11), Min/max discharge: Austin Creek (12), Min/max discharge: Russian River (13).

(1)	(2) (h)	(3) (mm)	(4) (cm)	(5) (m s^{-1})	(6) (deg)	(7) [cm (m s^{-1})]	(8) [cm (m s^{-1})]	(9) (mm h^{-1})	(10) (mm h^{-1})	(11) (%)	(12) (cms)	(13) (cms)
All (91)	20	44.3	2.69	12.8	216	32.5	471	2.21	4.09	28.8/35.1	5.7/31.6	55.6/159.5
Only cases with >45 mm in 96 h (60)	29	74.3	2.66	13.2	206	34.8	702	2.56	5.31	31.8/40.1	7.6/46.5	73.7/227.3
Seasonal: SON (22)	16	26.7	2.88	10.6	225	30.5	374	1.67	2.57	15.4/22.2	0.2/6.5	6.1/16.4
Seasonal: DJF (41)	22	62.4	2.56	13.3	209	34.1	565	2.84	5.50	37.2/45.6	9.3/54.0	84.5/265.6
Seasonal: MAM (23)	16	33.2	2.69	12.5	215	33.3	388	2.08	4.09	29.0/36.7	4.9/33.1	48.6/139.6
Duration: 8–15 h (60)	13	31.1	2.71	12.2	224	32.7	322	2.40	4.54	28.1/33.7	5.6/29.7	58.6/104.1
Duration: 16–23 h (15)	19	41.9	2.72	12.8	224	32.5	511	2.21	4.86	26.9/34.2	2.7/31.2	28.9/93.1
Duration: 24–31 h (6)	31	114.0	3.11	15.8	208	48.4	1055	3.68	8.04	25.9/40.5	1.7/56.5	22.8/241.0
Duration: >31 h (10)	40	142.2	2.90	16.1	223	45.0	1419	3.56	6.50	36.1/46.3	9.0/158.1	94.8/602.2

these 1460 samples for the forcing and impact variables. For example, comparison of the range of values of IWV with those of upslope wind speed (Figs. 4a,b) reveals how the upslope winds vary over a much wider dynamic range than does IWV. Also, Table 3 makes it possible to determine if a given measurement of upslope IWV flux is an extreme value, that is, a value greater than 50.8 cm (m s^{-1}) would represent conditions in the top 10% for that variable.

b. Seasonality of ARs and their impacts

Neiman et al. (2008a) used satellite observations to document the seasonality of ARs offshore based on IWV only. Their study showed that ARs occur in all seasons, but it also used the National Centers for Environmental Prediction–National Center for Atmospheric Research (NCEP–NCAR) reanalysis to show that the warm-season ARs were associated with weaker winds and less favorable orographic orientations and, ultimately, much less precipitation. Using the atmospheric river observatory (ARO) data from the current study, it was possible to assess the seasonality of ARs and their primary components and impacts. The cases were separated into seasons: December–February (DJF)—41 cases, March–May (MAM)—23 cases, June–August (JJA)—5 cases, and September–November (SON)—22 cases. Table 2 summarizes key characteristics of the composites for each season, excluding JJA because of its small sample size. DJF stood out as having the most ARs, the longest duration ARs with the strongest upslope winds, greatest IWV fluxes, maximum hourly rain rates (more than double those of SON and 34% greater than MAM), largest average rain rates, highest precursor soil moisture, maximum soil moisture (more than double those of SON and about 25% greater than MAM), and the largest streamflows. However, DJF cases had the lowest average maximum IWV value (i.e., 10% lower than in SON). Thus, the presence of stronger upslope winds overcame the somewhat smaller values of IWV associated with the cooler season. This result extends and refines conclusions from Neiman et al. (2008b) comparing summer and winter as derived from offshore reanalysis fields.

c. The role of AR duration in extreme events

Because streamflow is very sensitive to both hourly rain rates and long durations of relatively heavy rainfall that accompany most ARs, the observations are used here to assess the role of storm-total upslope water vapor transport during AR conditions in controlling storm-total AR rainfall and streamflow. The storm totals for each AR were obtained by time integrating the upslope IWV flux over the hours of AR conditions and calculating the rainfall accumulation at CZD during just

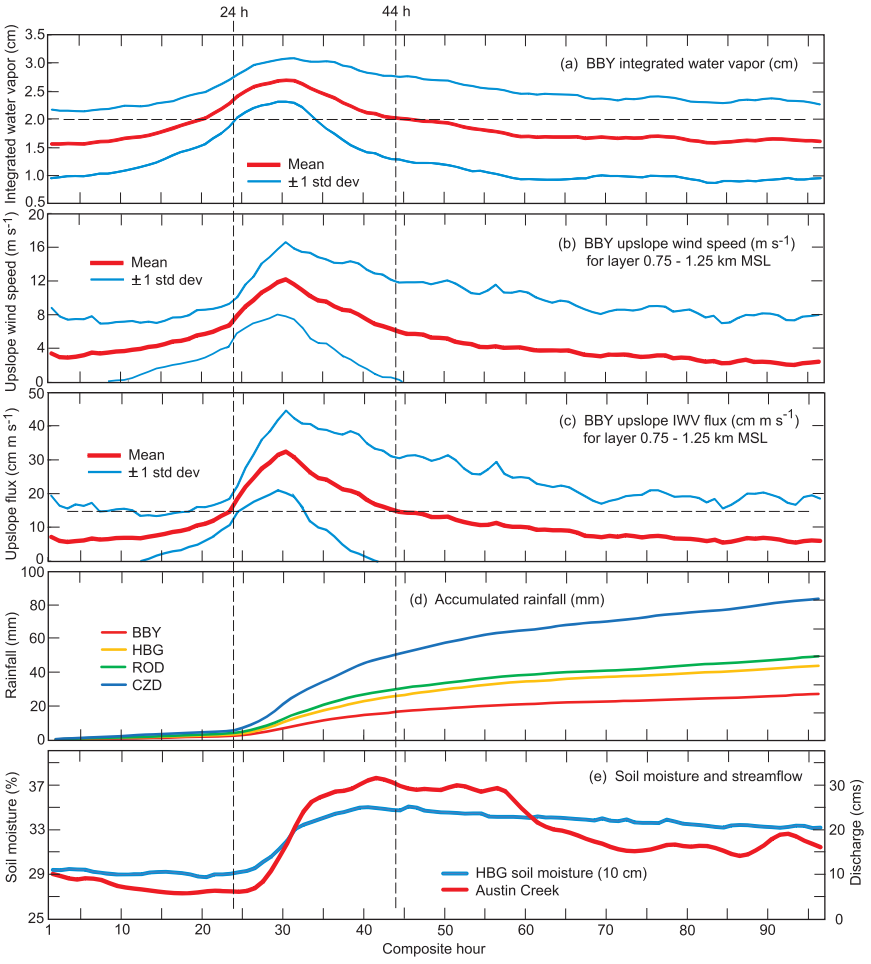

FIG. 3. (a)–(e) Composite time series of 91 AR events observed at the Bodega Bay ARO and nearby sites between 13 Nov 2004 and 8 Aug 2010. Vertical dashed lines at hours 24 and 44 mark the start and end times of composite AR conditions. The horizontal dashed lines in (a) and (c) represent threshold values of IWV (2 cm) and upslope IWV flux [15 cm (m s^{-1})] used in the study to define AR conditions. The "upslope" direction is toward 230°.

those hours. The resulting flux totals and precipitation totals are correlated with $r^2 = 0.75$ (Fig. 5a), by far the largest correlation found to date between precipitation and various measures of orographic forcing. For comparison, hourly upslope IWV fluxes and hourly CZD rainfall for the same cases are correlated with $r^2 = 0.49$. Although other methods of comparing time-integrated IWV flux with corresponding rainfall accumulation without AR criteria were attempted, none achieved the level of correlation found using the AR criteria to define events.

Similarly, the storm-total upslope IWV fluxes can be compared with the ensuing storm-total volume of streamflow in nearby Austin Creek during AR hours (Fig. 5b). Remarkably, more than 61% of the variation in the streamflow volume is associated with the amount of atmospheric water vapor transported up the slope during atmospheric-river conditions. Further, by considering the precursor soil moisture conditions (i.e., at hour 23 of the composite 96-h-long time series), it is clear that the streamflow volume was less than expected when the soil was initially dry (Fig. 5b); quantitatively, the precursor soil moisture conditions accounted for an additional 17% of the variance in storm-total streamflow (calculated by correlating streamflow and soil moisture directly), raising the total streamflow variance captured to 79%. In contrast, when the storm-total streamflow volume is compared to the storm-total precipitation, the variance captured is 71%.

To clarify the role of AR duration in modulating these relations, the 91 cases are stratified into four duration categories: 8–15 h (60 cases), 16–23 h (15 cases),

24–31 h (6 cases), and >31 h (10 cases), with results shown in Table 2 and Figs. 5a and 6.[4] Comparison of the composite streamflow from the 10 longest events, which have a composite average duration of 40 h (Table 2), to the composite of all 91 events, which have a composite average duration of 20 h (Table 2), reveals the impacts associated with ARs that had double the duration of typical ARs.

The most relevant measure of impact on streamflow is the difference between the peak discharge during the composite event and lowest discharge beforehand (Table 2). For AR events that lasted twice as long on average, Austin Creek rose by 149.1 cms for the longest events and only 25.9 cms for all events on average, a factor of 5.8 greater rise. Similarly for the Russian River, the rises were 507.4 and 103.9 cms, respectively, a factor of 4.9 greater rise. Because the composite average duration of the 15 events that lasted 16–23 h was 19 h, it also represents a sample for which the composite average duration was roughly half that of the 10 longest events, a similar comparison of streamflow rises can be made. This is a useful comparison since these two samples (i.e., cases with duration >31 h versus cases with duration of 16–23 h) have no overlapping cases at all. In this comparison the Austin Creek rise was 5.2 times greater and the Russian River rise was 7.9 times greater. Averaging these four results indicates that, on average, the rivers rose 6 times more for the 10 longest events than for those with composite average duration that was roughly half as long (i.e., 20 and 19 h versus 40 h).

The enhanced impact of the longer duration (doubled) events is due to greater storm-total water vapor transport, larger rain rates, larger storm-total precipitation, wetter precursor soil moisture, and greater increase in soil moisture during a storm (Table 2, Fig. 6). The longest duration events averaged 1419 cm (m s^{-1}) of storm-total upslope IWV flux versus 471 cm (m s^{-1}) for all 91 events [511 cm (m s^{-1}) for the 16–23 h duration events], roughly a factor of 3 greater water vapor transports up the mountain slope. This increase was not only the result of longer duration alone but also stronger maximum upslope winds (26% stronger relative to either all 91 cases or to the 16–23 h duration events) and larger maximum IWV values (7%–8% greater). The precursor soil moisture conditions are wettest for the longest duration class (36.1% versus 28.8% and 26.9%, Table 2), and the average increase in soil moisture during the storm is greater for the >31 h events (10.2%) than for all events (6.3%) and for the events lasting 16–23 h (7.3%). All 10 of the longest duration events were in DJF, a period that routinely had higher precursor soil moistures, as seen in the seasonality composites (Table 2).

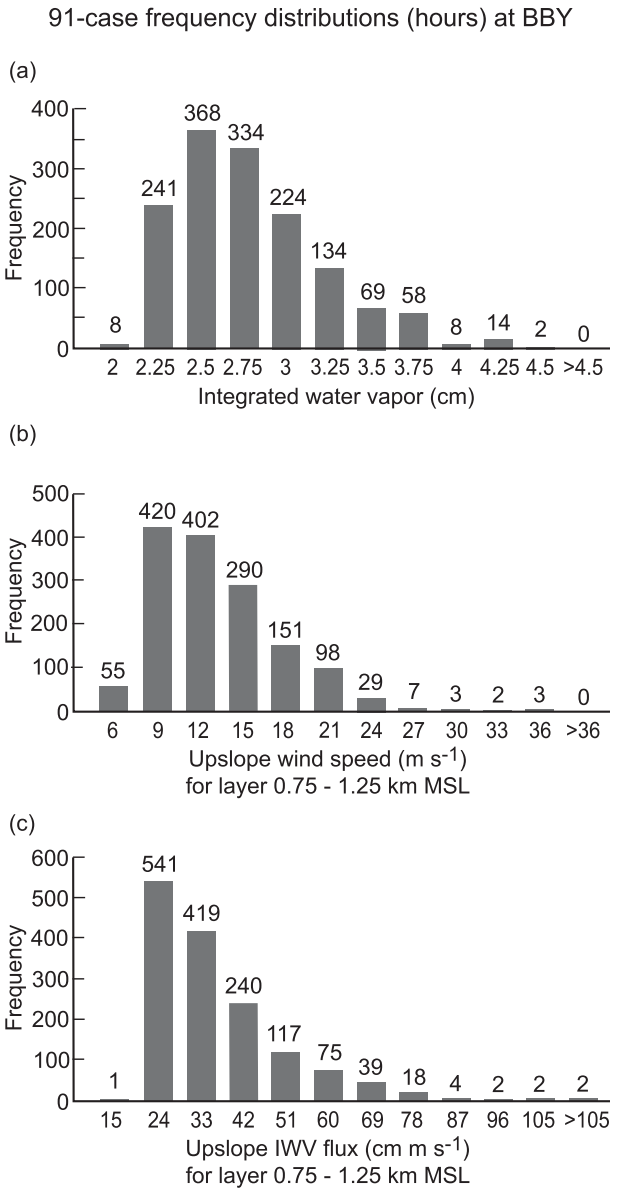

FIG. 4. Histograms showing the frequency distribution of hourly observations of (a) IWV, (b) upslope wind speed, and (c) upslope IWV flux during the 1460 h of AR conditions within the 91 AR events.

[4] As would be expected from visual inspection of Fig. 6, the Student's *t* test (one sided) revealed that the composite results for these duration categories are statistically significant at >90% confidence level in their difference from a few hours after onset of AR conditions, until near the end of AR conditions. In addition, for the streamflow and soil moisture prior to AR onset, the longest-duration events are statistically more moist and have greater streamflow than the shorter-duration events. Interestingly, all events are statistically similar in terms of the atmospheric forcings prior to and within the first hours of AR conditions.

TABLE 3. Upper 10% and 1% thresholds for hourly values of each key variable from within the 1460 AR hours during the 6-yr study period.

	Top 10% threshold	Top 1% threshold
Integrated water vapor (cm)	3.3	4.1
Total wind speed (m s^{-1})	22.2	30.6
Total integrated water vapor flux [cm (m s^{-1})]	61.0	83.0
Upslope wind speed (m s^{-1})	17.9	24.0
Upslope integrated water vapor flux [cm (m s^{-1})]	50.8	74.4
CZC rain rate (mm)	8.7	16.0
HBG soil moisture	51.6%	56.8%
Russian River streamflow (cms)	376.6	1044.9
Austin Creek streamflow (cms)	115.9	341.7

Four of the 10 longest events started within less than 48 h of the end of the previous AR (Table 1); that is, they seem to be part of ''families'' of ARs that occur in rapid succession. The average rain rates are roughly 50% higher for the two longest duration classes (Table 2). Finally, the maximum hourly rain rates during the events are greater in composites of the longer two classes than the shorter two. Taken together, the longest ARs contribute disproportionately to total precipitation. Roughly 25% of all precipitation at CZD over six years came from the 16 longest ARs during a total of 586 h (1.17% of all hours studied).

4. Conclusions

Past studies (see section 1) have shown that, when AR conditions strike coastal mountains in California, the storm-total precipitation is dictated in large part by the strength of the atmospheric river (i.e., low-level winds and water vapor content), its width, orientation of the wind relative to mountains, and the AR's overall propagation (Fig. 7a). But, by adding information regarding the duration of AR conditions and factoring in the seasonality of precursor conditions, it is also possible to identify the events that produced the most extreme storm-total precipitation and, ultimately, the

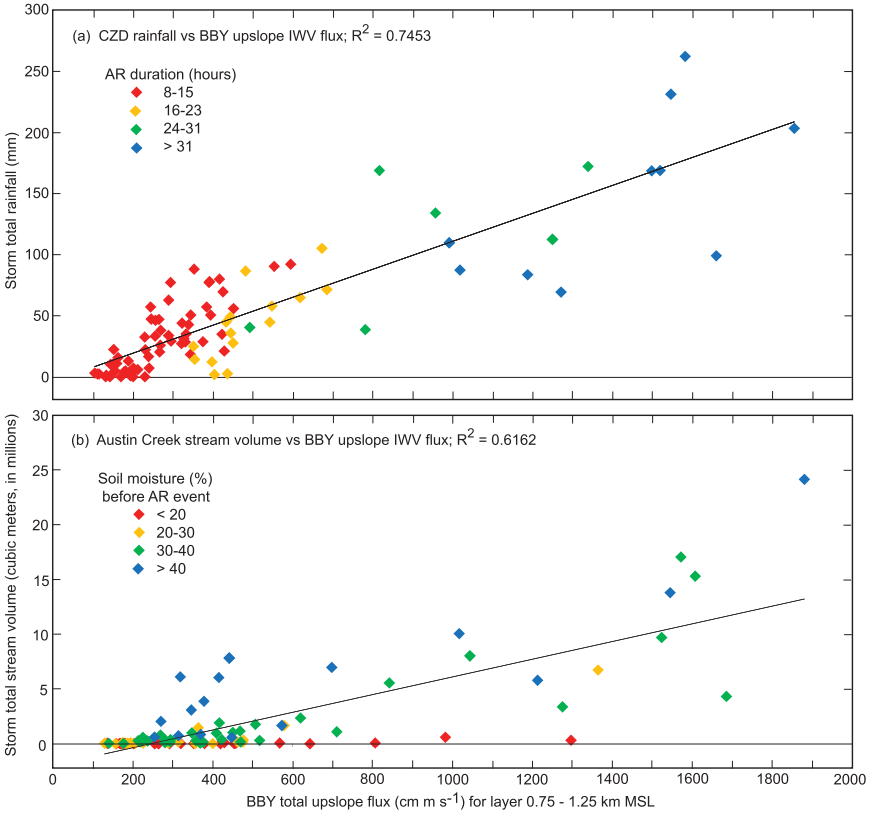

FIG. 5. (a) Scatterplot of storm-total precipitation at CZD vs storm-total upslope IWV flux at BBY during AR conditions for the 91 cases (color coded by AR duration). (b) Scatterplot of the volume of runoff in Austin Creek during AR conditions vs storm-total upslope IWV flux at BBY during AR conditions for the 91 cases (color coded by precursor soil moisture conditions). The correlation (R^2) is shown for each panel.

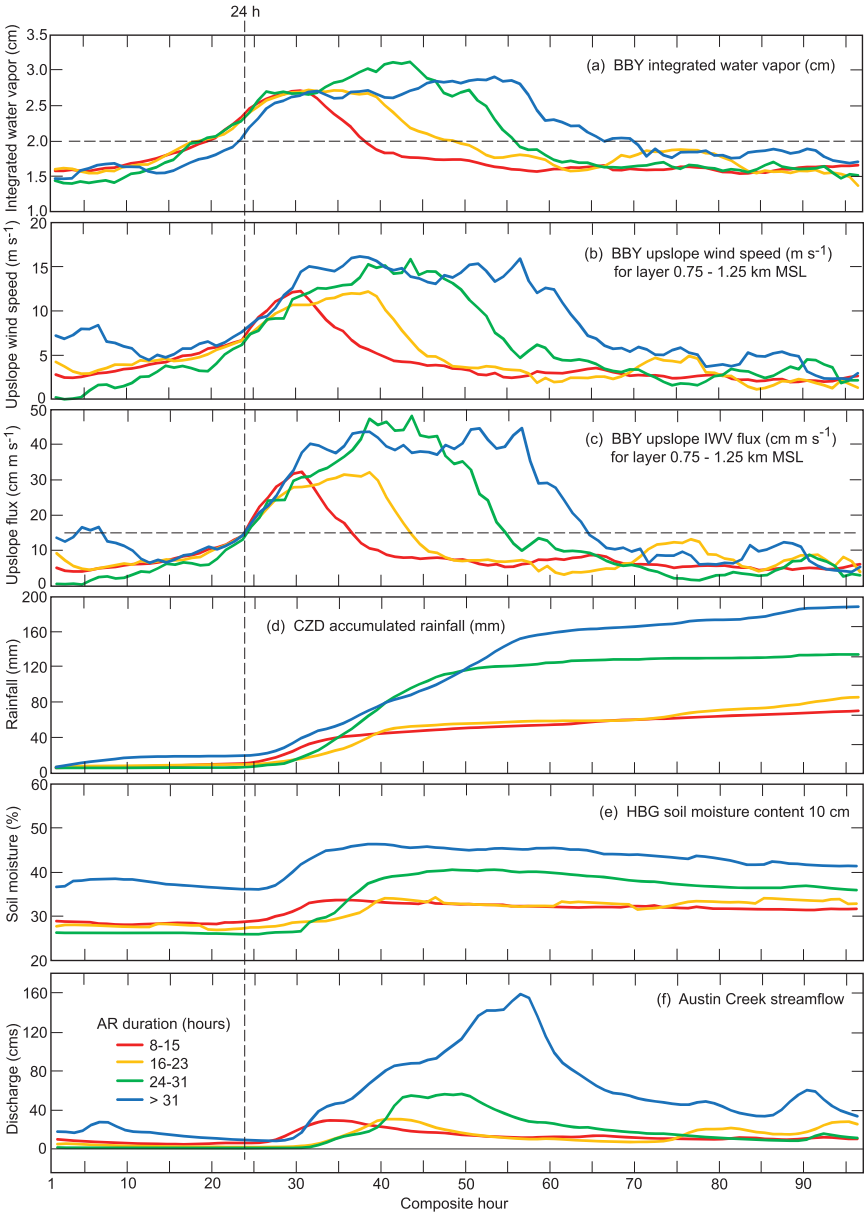

FIG. 6. Composite time series of AR events stratified by AR duration, that is, 8–15 h (red), 16–23 h (yellow), 24–31 h (green), and >31 h (blue). The vertical dashed line at hour 24 marks the start of composite AR conditions.

highest streamflows (Fig. 5b). It is remarkable that the compositing was conditioned only on atmospheric characteristics here. The fact that objective criteria were able to distinguish the events that were most extreme hydrologically, *without conditioning the case selections on either the observed precipitation or on the streamflow*, indicates that the criteria developed here have the potential to be especially useful in prediction of extreme events. These results help inform forecasting systems of what variables to focus on and how to interpret them. This is a particularly useful finding because the models used in long-lead forecast strategies represent the large-scale atmospheric conditions used here more directly than the more surficial outcomes (precipitation and streamflow).

For example, if forecast models show IWV $>$ 2 cm, with IWV fluxes greater than 15 cm (m s^{-1}), both lasting for 32 h or longer, then extreme precipitation is likely to occur. If, in addition, the soil moisture is >35% at representative sites, one should expect streamflows in the top few percent of all cases. These findings will be used by HMT to develop forecasting tools, which can

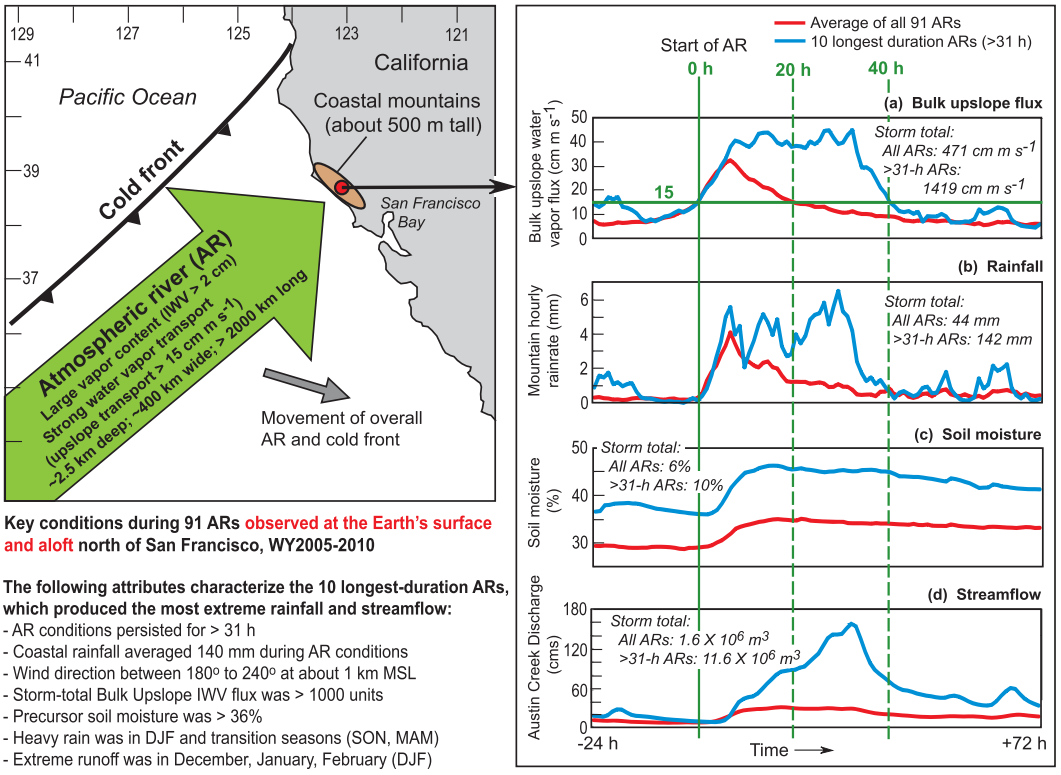

FIG. 7. Schematic summary of atmospheric and hydrometeorological conditions associated with landfalling atmospheric rivers recorded by an ARO at Bodega Bay and additional observations from nearby. (left) Plan view (based on previous studies summarized in section 1) of an AR striking the coast ahead of a cold front (see Fig. 1a for an example). Note that the storm systems tend to move from roughly west to east across the observing site (red dot), with winds blowing from southwest to northeast. (right) Composite time series traces comparing the 10 longest-lasting ARs (in terms of time affecting the field site) vs the composite of all 91 cases. The 10 ARs that lasted longest over the field site averaged twice as long (40 h) as the average AR event (20 h). (a)–(d) The solid (dashed) vertical green lines mark the start time (end times) of composite AR conditions. The horizontal green line in (a) shows the upslope IWV flux threshold, 15 cm (m s^{-1}), for AR conditions.

take advantage of a modern statewide observing network for monitoring AR conditions and precursor soil moisture being implemented in California. It is anticipated that these results can impact precipitation forecasting. They could also be used in flood prediction through incorporation into a statistical streamflow modeling framework to diagnose and forecast various aspects of extreme flow events, for example, using a generalized linear modeling and extreme value analysis framework. These could offer new management alternatives for storm- and flood-related societal, environmental, and economic challenges in the region. Future work that is needed to enable such impacts include studies of conditions that lead to long-duration AR events, such as mesoscale frontal waves (e.g., Neiman et al. 2004; Ralph et al. 2011), and the role of entrainment of tropical water vapor into some ARs (e.g., Bao et al. 2006; Stohl et al. 2008; Ralph et al. 2011).

Results from this study are also expected to be representative of behavior elsewhere on the U.S. West Coast and in other regions of the world where ARs have been shown to be important in extreme precipitation and flooding, including western Europe, the Chilean Andes, and the southeastern United States. Parts of New Zealand, southeast Alaska, and western Canada may also be affected by similar storms.

Acknowledgments. This paper would not have been possible without the sustained collection of observations at several field sites operated by the talented and dedicated NOAA Physical Sciences Division engineering staff.

REFERENCES

Bao, J.-W., S. A. Michelson, P. J. Neiman, F. M. Ralph, and J. M. Wilczak, 2006: Interpretation of enhanced integrated water vapor bands associated with extratropical cyclones: Their formation and connection to tropical moisture. *Mon. Wea. Rev.*, **134,** 1063–1080.

Carter, D. A., K. S. Gage, W. L. Ecklund, W. M. Angevine, P. E. Johnston, A. C. Riddle, J. S. Wilson, and C. R. Williams,

1995: Developments in UHF lower tropospheric wind profiling at NOAA's Aeronomy Laboratory. *Radio Sci.,* **30,** 997–1001.

Dettinger, M., 2011: Climate change, atmospheric rivers, and floods in California—A multimodel analysis of storm frequency and magnitude changes. *J. Amer. Water Resour. Assoc.,* **47,** 514–523, doi:10.1111/j.1752-1688.2011.00546.x.

——, F. M. Ralph, T. Das, P. J. Neiman, and D. Cayan, 2011: Atmospheric rivers, floods, and the water resources of California. *Water,* **3,** 455–478.

——, and Coauthors 2012: Design and quantification of an extreme winter storm scenario for emergency preparedness and planning exercises in California. *Nat. Hazards,* **60,** 1085–1111.

Duan, J. M., and Coauthors, 1996: GPS meteorology: Direct estimation of the absolute value of precipitable water. *J. Appl. Meteor.,* **35,** 830–838.

Guan, B., N. P. Molotch, D. E. Waliser, E. J. Fetzer, and P. J. Neiman, 2010: Extreme snowfall events linked to atmospheric rivers and surface air temperature via satellite measurements. *Geophys. Res. Lett.,* **37,** L20401, doi:10.1029/2010GL044696.

Jankov, I., J.-W. Bao, P. J. Neiman, P. J. Schultz, Y. Huiling, and A. B. White, 2009: Evaluation and comparison of microphysical algorithms in ARW-WRF model simulations of atmospheric river events affecting the California coast. *J. Hydrometeor.,* **10,** 847–870.

Lavers, D. A., R. P. Allan, E. F. Wood, G. Villarini, D. J. Brayshaw, and A. J. Wade, 2011: Winter floods in Britain are connected to atmospheric rivers. *Geophys. Res. Lett.,* **38,** L23803, doi:10.1029/2011GL049783.

Leung, L. R., and Y. Qian, 2009: Atmospheric rivers induced heavy precipitation and flooding in the western U.S. simulated by the WRF regional climate model. *Geophys. Res. Lett.,* **36,** L03820, doi:10.1029/2008GL036445.

Mattioli, V., E. R. Westwater, C. Cimini, J. S. Liljegren, B. M. Lesht, S. I. Gutman, and F. J. Schmidlin, 2007: Analysis of radiosonde and ground-based remotely sensed PWV data from the 2004 North Slope of Alaska Arctic Winter Radiometric Experiment. *J. Atmos. Oceanic Technol.,* **24,** 415–431.

Moore, B. J., P. J. Neiman, F. M. Ralph, and F. Barthold, 2012: Physical processes associated with heavy flooding rainfall in Nashville, Tennessee, and vicinity during 1–2 May 2010: The role of an atmospheric river and mesoscale convective systems. *Mon. Wea. Rev.,* **140,** 358–378.

Neiman, P. J., F. M. Ralph, A. B. White, D. A. Kingsmill, and P. O. G. Persson, 2002: The statistical relationship between upslope flow and rainfall in California's coastal mountains: Observations during CALJET. *Mon. Wea. Rev.,* **130,** 1468–1492.

——, P. O. G. Persson, F. M. Ralph, D. P. Jorgensen, A. B. White, and D. A. Kingsmill, 2004: Modification of fronts and precipitation by coastal blocking during an intense landfalling winter storm in Southern California: Observations during CALJET. *Mon. Wea. Rev.,* **132,** 242–273.

——, F. M. Ralph, G. A. Wick, Y.-H. Kuo, T.-K. Wee, Z. Ma, G. H. Taylor, and M. D. Dettinger, 2008a: Diagnosis of an intense atmospheric river impacting the Pacific Northwest: Storm summary and offshore vertical structure observed with COSMIC satellite retrievals. *Mon. Wea. Rev.,* **136,** 4398–4420.

——, ——, ——, J. Lundquist, and M. D. Dettinger, 2008b: Meteorological characteristics and overland precipitation impacts of atmospheric rivers affecting the west coast of North America based on eight years of SSM/I satellite observations. *J. Hydrometeor.,* **9,** 22–47.

——, A. B. White, F. M. Ralph, D. J. Gottas, and S. I. Gutman, 2009: A water vapor flux tool for precipitation forecasting. *Proc. Inst. Civ. Eng.: Water Manage.,* **162,** 83–94.

——, E. M. Sukovich, F. M. Ralph, and M. Hughes, 2010: A seven-year wind profiler–based climatology of the windward barrier jet along California's northern Sierra Nevada. *Mon. Wea. Rev.,* **138,** 1206–1233.

——, L. J. Schick, F. M. Ralph, M. Hughes, and G. A. Wick, 2011: Flooding in western Washington: The connection to atmospheric rivers. *J. Hydrometeor.,* **12,** 1337–1358.

Peixoto, J. P., and A. H. Oort, 1992: *Physics of Climate.* American Institute of Physics, 520 pp.

Ralph, F. M., and M. D. Dettinger, 2012: Historical and national perspectives on extreme West Coast precipitation associated with atmospheric rivers during December 2010. *Bull. Amer. Meteor. Soc.,* **93,** 783–790.

——, P. J. Neiman, D. E. Kingsmill, P. O. G. Persson, A. B. White, E. T. Strem, E. D. Andrews, and R. C. Antweiler, 2003: The impact of a prominent rain shadow on flooding in California's Santa Cruz mountains: A CALJET case study and sensitivity to the ENSO cycle. *J. Hydrometeor.,* **4,** 1243–1264.

——, ——, and G. A. Wick, 2004: Satellite and CALJET aircraft observations of atmospheric rivers over the eastern North Pacific Ocean during the El Niño winter of 1997/98. *Mon. Wea. Rev.,* **132,** 1721–1745.

——, and Coauthors, 2005: Improving short-term (0–48 hour) cool-season quantitative precipitation forecasting: Recommendations from a USWRP workshop. *Bull. Amer. Meteor. Soc.,* **86,** 1619–1632.

——, P. J. Neiman, G. A. Wick, S. I. Gutman, M. D. Dettinger, D. R. Cayan, and A. B. White, 2006: Flooding on California's Russian River: Role of atmospheric rivers. *Geophys. Res. Lett.,* **33,** L13801, doi:10.1029/2006GL026689.

——, E. Sukovich, D. Reynolds, M. Dettinger, S. Weagle, W. Clark, and P. J. Neiman, 2010: Assessment of extreme quantitative precipitation forecasts and development of regional extreme event thresholds using data from HMT-2006 and COOP observers. *J. Hydrometeor.,* **11,** 1288–1306.

——, P. J. Neiman, G. N. Kiladis, K. Weickman, and D. W. Reynolds, 2011: A multi-scale observational case study of a Pacific atmospheric river exhibiting tropical–extratropical connections and a mesoscale frontal wave. *Mon. Wea. Rev.,* **139,** 1169–1189.

Smith, B. L., S. E. Yuter, P. J. Neiman, and D. E. Kingsmill, 2010: Water vapor fluxes and orographic precipitation over northern California associated with a land-falling atmospheric river. *Mon. Wea. Rev.,* **138,** 74–100.

Stohl, A., C. Forster, and H. Sodemann, 2008: Remote sources of water vapor forming precipitation on the Norwegian west coast at 60°N—A tale of hurricanes and an atmospheric river. *J. Geophys. Res.,* **113,** D05102, doi:10.1029/2007JD009006.

Viale, M., and M. N. Nuñez, 2011: Climatology of winter orographic precipitation over the subtropical central Andes and associated synoptic and regional characteristics. *J. Hydrometeor.,* **12,** 481–507.

White, A. B., and Coauthors, 2012: NOAA's rapid response to the Howard A. Hanson Dam flood risk management crisis. *Bull. Amer. Meteor. Soc.,* **93,** 189–207.

Zamora, R. J., F. M. Ralph, E. Clark, and T. Schneider, 2011: The NOAA Hydrometeorology Testbed soil moisture observing networks: Design, instrumentation, and preliminary results. *J. Atmos. Oceanic Technol.,* **28,** 1129–1140.

Zhu, Y., and R. E. Newell, 1998: A proposed algorithm for moisture fluxes from atmospheric rivers. *Mon. Wea. Rev.,* **126,** 725–735.